Year of emergence of ocean acidification in the Global Ocean

Hongjie Wang[1,*], Li-Qing Jiang[2], Brendan R. Carter[3,4], Wei-Jun Cai[1]

1. School of Marine Science and Policy, University of Delaware, Newark, DE, United States

2. Earth System Science Interdisciplinary Center, University of Maryland, College Park, MD, United States

3. Joint Institute for the Study of the Atmosphere and Ocean, University of Washington, Seattle, WA, United States

4. Pacific Marine Environmental Laboratory, National Oceanic and Atmospheric Administration, Seattle, WA, United States

MS prepared for *Global Biogeochemical Cycles*

*Correspondence to Dr. Hongjie Wang (hwangde@udel.edu)

Key Points (3 max, < 100 characters each)

1. pCO_2, pH and Ω changes have fully emerged from preindustrial condition in the open ocean, but not in ocean margins yet.
2. pCO_2, pH and Ω changes will fully emerged from present conditions between year 2040 ~2060 in global ocean.
3. Year of emergence for Ω is ~30 years later than for pCO_2 and pH in the open ocean.

Abstract

Year of emergence (YoE) is the year when an environment and the organisms within begin to experience significant different conditions (two times of natural variability) from the pre-industrial conditions (~1770 C.E.). This study calculates the global surface ocean YoEs for pH, partial pressure of CO_2 (pCO_2) and aragonite saturation (Ω) from a recent calculated surface ocean carbonate chemistry data product. The data product is calculated from the Surface Ocean CO_2 Atlas version 6 (SOCATv6) with modeled pCO_2 changes in the global surface ocean from the ESM2M model. We find that pCO_2, pH and Ω generally emerged from preindustrial conditions in the open ocean by the year 1950, while these properties have still not yet emerged along many ocean margins. We also find that Ω had a significantly delayed YoE compared to pH and pCO_2. The delayed YoE for Ω is caused by its lasting sensitivity to temperature variability, which increases the natural variability experienced by organisms, and a partial cancellation of the long term acidification trend by the global warming. Together, YoEs presented here highlight that there are hotspots (open ocean) and coldspots (ocean margins that were impacted by boundary currents) for the emergence of anthropogenic signals. Continuous data collection and synthesis are needed to further examine the impact of ocean acidification on ecosystem health.

Keywords

Year or Emergence; Ocean Acidification; Buoys; Surface Ocean CO_2 Atlas Version 6; ESM2M Model

1. Introduction

Year of emergence (YoE) is date at which the change from an anthropogenic climate signal exceeds the natural variability of the unperturbed system (Hawkins & Sutton, 2012; Keller et al., 2014). Practically, it is defined as the year when observed value exceeds the historical ranges persistently for the remainder of the time series (Henson et al., 2017). Therefore, YoE is a function of both natural variability and the external climate signal: smaller climate forcing and higher natural variability correspond to delayed YoE and *vice versa*. YoE is commonly applied in climate science to predict when anthropogenic forcing become meaningful relative to natural variability, for example, sea-level rise, precipitation changes, and temperature changes (Crompton et al., 2011; Giorgi & Bi, 2009; Hawkins & Sutton, 2012; Lee et al., 2016; Lyu et al., 2014; Sui et al., 2014).

YoE is closely related to "times of emergence (ToE)," which represents the length of time for a trend to push a natural system beyond the ranges experienced at the outset of a model simulation or observation effort, as opposed to during the preindustrial era for YoE. With this definition, YoE is absolute whereas ToE is specific to a given time window which must be specified. YoE is different also from the "time of detection," which is the minimum length of a record required for detection of an external climate signal from the specified beginning of an observational record. When measurement uncertainty is not a limitation, frequently-measured climate change signals can sometimes be detected before systems have fully emerged from their envelopes of natural variability because data treatments, such as "deseasonalization," can average out some timescales of variability (Carter et al., 2019). More recently, the YoE concept has been applied to study biogeochemical responses to anthropogenic forcing, for example, ocean acidification, which refers to the decreasing pH and calcium carbonate mineral saturation states (Ω) that results from continuous ocean anthropogenic CO_2 absorption (Feely et al., 2009).

Based on a biogeochemical model, Friedrich et al. (2012) reported that the present surface water Ω has already exceeded the level of natural variability since the mid-twentieth century in vast areas of the global oceans. Ricke et al. (2013) further concluded that all existing coral reefs would be surrounded by mean Ω well outside of preindustrial (or even present day) conditions (Ωarag<3.5) by the end of this century under the IPCC business-as-usual CO_2 emission scenario. To make it more comparable, Keller et al. (2014) showed that the climate signals in ocean biogeochemical properties (pCO_2, pH, and dissolved inorganic carbon) emerge from modern conditions on much shorter timescales (10~30 years) than signals in physical marine properties (i.e., sea surface temperature, 45~90 years). However, the Earth System Models in previous studies tended to underestimate natural variability, especially in coastal areas, since coarser-resolution non-eddy-resolving models do not capture small-scale biogeochemical processes (Sutton et al., 2016). Thus, such Earth system model outputs risk understimating YoE from human-induced climate signals due to underestimation of the noise (natural variability) and overestimation of climate signal-to-noise ratios.

Some recent work started to examine ToEs based on different kinds of *in-situ* observations. With the aid of high-frequency autonomous mooring stations, Sutton et al. (2016) found both pH and Ω have already fallen outside of bounds of preindustrial variability in the open ocean, while the high natural variabilities in coastal areas maintain the overlap between present and preindustrial carbonate chemical conditions. The latest study by Turk et al. (2019) also showed a high spatial variability of ToEs for fCO_2 (23±13 years) when starting from ~1990 in north American margins. Their highest value was found around the northeastern U.S. Continental and Scotian Shelves where the increasing surface primary productivity counteracts ocean

84 acidification. However, YoEs of oceanic CO_2, pH, and Ω has not been explored broadly
85 throughout the ocean using observation-based quantifications of natural property ranges.

86 This study first presents YoE estimates in the global ocean to show when anthropogenic CO_2
87 uptake first caused ocean acidification changes exceed the preindustrial variability and present
88 conditions. We then discuss the oceanographic and thermodynamic causes of YoE differences in
89 various regions. Findings from this study will provide explicit information for both decision-
90 makers and stakeholders regarding the hotspots and coldspots of ocean acidification.

91 **2. Datasets and Noise Calculation**

92 This analysis is based on a recent data product combining observed surface ocean pH
93 calculated from the 6th Version of the Surface Ocean CO_2 Atlas (SOCATv6, 1991-2018, ~23
94 million observations) with modeled pCO_2 trajectories at individual locations of the global surface
95 ocean from the ESM2M model (Jiang et al., 2019). Modern pH and Ω were calculated from the
96 SOCATv6 with CO2SYS (in Matlab (van Heuven, 2011)) based on fCO_2 and salinity derived A_T
97 (Carter et al., 2017). The uncertainty for pH and Ω is 0.01 and 0.13, respectively. For details of
98 the data product, please refer to Jiang et al. (2019).

99 The SOCATv6 data product was also used to estimate carbonate chemistry variability. In
100 SOCATv6, some coastal areas, such as the Japanese, western European and North American
101 margins generally have better data coverage, and the number of sampling points is about one
102 order of magnitude higher than in open ocean given recent years' data collections (Fig. S8). To
103 avoid impacts from sampling gaps and summer sampling biases, SOCATv6 based-natural
104 variability or *Noise* was only calculated in grids (at resolution of 1° latitude by 1° longitude) that

had enough data: the minimum amount of data to be included was 5 years with at least 8 months sampled from any 10 year span. For these grid cells, the outliers in each grid were removed to avoid the impact of short time extreme values (outliers were defined as values more than 1.5 times interquartile range above (below) the third (first) quartile). We then detrended the dataset in each grid with an average oceanic rate of 1.89 µatm yr^{-1} for fCO_2, -0.0018 yr^{-1} for pH and -0.0078 yr^{-1} for Ω from 1980s to 2010s (Bates et al., 2014). The standard deviation of this detrended time series (VARsocat, hereafter) represents a combination of all daily, sub-seasonal, seasonal, interannual, and decadal variability in each grid cell. Some variability estimate uncertainly is inevitable due to incomplete representations of some timescales of variability (notably decadal).

The spatial coverage of SOCATv6 data is biased towards the Northern Hemisphere due to the availability of cruise opportunities (Fig. S8). To better understand the *Noise* pattern in the global ocean we also calculated YoEs based on the data product developed by Jiang et al. (2019). We selected three subsets of the model output: (1) from 1770 to 1870, (2) from 1990 to 2020, and (3) from 2020 to 2050 to quantify the historical, present, and future ocean acidification trends. We then detrended the subset from 1990 to 2020 with the modeled *in situ* present trends. Finally, the standard deviation of detrended sub-dataset (from 1990 to 2020) was calculated to represent the model-based variability (VARmodel). Derived from monthly-averages of 1°x1° gridded output, this variability mostly reflects seasonal and decadal variabilities.

Our third means of estimating variability relies on the fixed time-series mooring dataset (Sutton et al., 2019). This dataset encompasses the most complete record of natural variability from diurnal to decadal time scales. The highly temporally-resolved buoy observations (~3

hourly) were used as reference stations to scale the natural variability inferred from the ESM2M model. The 38 buoy sites in the data products are located in a variety of environments including the open ocean, the coastal ocean, and in coral reefs, though only three of them are from the Southern Hemisphere. Surface A_T for each buoy site was calculated with the same method (LIARv2) as for SOCATv6, then both surface Ω and pH was calculated based on pCO_2 and estimated A_T, again using CO2SYS. The outliers in each site were also removed from raw data to get a "clean" dataset. Most buoy sites have a record that is too short (<12 years) to fully-resolve a long term trend (Sutton et al., 2019), but we still detrended all mooring site with the same ocean acidification rates as for SOCATv6 dataset to avoid the bias caused by record length differences. The standard deviation of the detrended "clean" dataset (VARbuoys) was then calculated to represent the "full" variability in each buoys site. Note that, given that the difference between fCO_2 and pCO_2 is minor (<0.4%, Zeebe & Wolf-Gladrow (2001)), we ignored their difference when comparing the deviations between the above three datasets.

3. Year of Emergence Calculation

In this study, our focus is to quantify when the system will experience a new condition that persistently exceeds the envelope of natural variability around the selected initial condition. Including the full variability is important to assess ecological consequences of ocean acidification, such as, to predict when ocean acidification will surpass biologically relevant thresholds in the future. Thus, we calculated YoE as the first year when the projected state of an interested variable crosses a pre-defined baseline for emergence (2× *Noise)*, which represents the anthropogenic caused change exceeds over 95% confidence interval of background variability (Keller et al., 2014).

Noise is derived with three different methods from the global natural variability (VAR) estimates, which are calculated as explained in Section 2 for SOCATv6 (VARsocat), the ESM2M model output (VARmodel) as adapted by Jiang et al. (2019), and moored buoys (VARbuoys). Given that VARmodel was calculated from monthly averaged model output, VARmodel tends to underestimate natural variability, thus, we cross-checked the variabilities from all three datasets, and applied adjustments to VARmodel to scale it to better match corresponding VARsocat and VARbuoys estimates. For Method 1 we scaled VARmodel based on the relationship between VARmodel and VARsocat (detailed information in Section 4.1). The second and third methods for scaling VARmodel were based on empirical relationships between VARmodel and VARbuoys fit to water column depth and sea surface temperature variability (see detail information in supplementary information). Sea surface temperature (SST) variability was inferred globally from satellite SST products (http://orca.science.oregonstate.edu/1080.by.2160.monthly.hdf.sst.modis.php) and depth was interpolated from ETOPO1 1 Arc-Minute Global Relief Model (Amante & Eakins, 2009) to allow a global reconstruction with these fits. The three sets of variabilities products for pCO_2, pH and Ω are reported in supplementary information.

An early study reported that the increase of atmospheric pCO_2 enhances the seasonal surface ocean pCO_2 variability amplitude at a rate of 0.0~0.4 μatm yr^{-1} from 1980s to 2010s (Landschützer et al., 2018). This implies the natural variability of inorganic carbon should increase over time. However, we assume that the *Noise*, or the adjusted VARmodel, was unchanging over the entire time series. As *Noise* is inferred from the larger modern variability—and YoEs tend to be historical dates for carbonate chemistry properties—we contend this potential error is likely to bias YoEs to more recent dates on average, though the reverse could be

true for YoEs that are calculated to be after the modern date or any ToEs calculated for future changes. We then fit a fifth-order polynomial (*f*(year)) against year to predict pCO_2, pH and Ω time series in each 1° latitude by 1° longitude grid (Fig. 1). YoE is calculated as the year, when *f*(year)) - *Noise* > *f*(1770)+ *Noise*, which represents the YoE from the preindustrial conditions present when climate change started. We also calculated ToE_2020, which was defined as the year, when *f*(year)) -*Noise* > *f*(2020)+*Noise*, which represents the ToE from present conditions. In the main text, we report the YoEs based on first VARmodel adjustment method. The other two sets of YoEs and ToE_2020s are reported in supplementary information. We contend the spatial distributions of YoEs by the three *Noise* adjustment methods are qualitatively similar, with an average standard deviation between the three estimates for each grid cell of 14~18 years (Fig. S6), and a much smaller standard deviation of 2~5 years for ToE_2020s (Fig. S7).

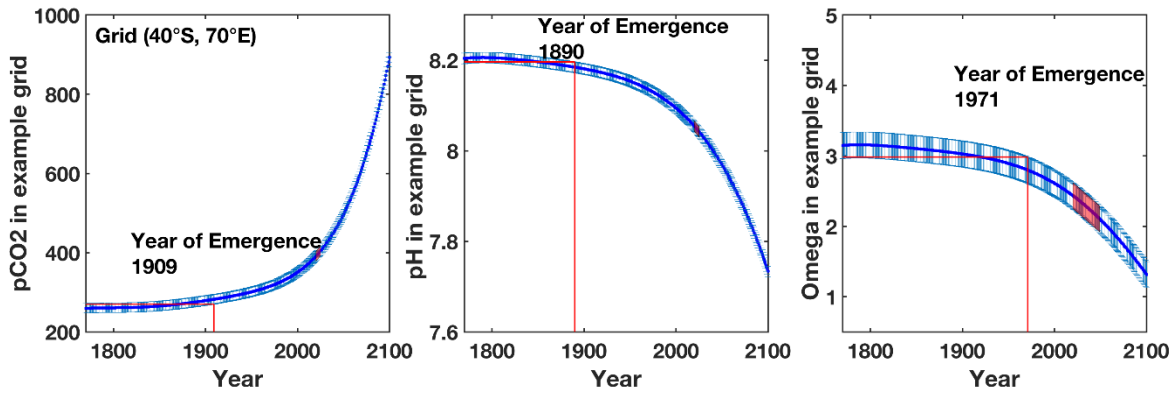

Fig. 1. Method to calculate year of emergence in one example grid (40°S, 70°E) for pCO_2, pH and Ω. The horizontal lines show when the 95% confidence interval fully emerges from the preindustrial condition (year 1770) (e.g., in panel c when the +1σ window value equals the initial -1σ window value). The red patches show the time of emergence from present states (year 2020).

4. Result and Discussion

4.1 ESM2M Model Variability Adjustment

Both VARmodel and VARsocat are close to VARbuoys in open ocean. Thus, both the ESM2M model and SOCATv6 capture natural variability adequately in open ocean. This good relationship results from the dominant role of seasonal variability and interannual variability to total variability in open ocean (see: discussion in supplementary information). Furthermore, VARmodel can approximately explain 62%, 63% and 82% of VARsocat for pCO_2, pH and Ω in global scale (Fig. 2). Thus, with the relationships in Fig. 2, we adjusted VARmodel to get more realistic variabilities on a global scale and to derive YoEs beyond the spatial area covered by SOCATv6.

Both SOCATv6 and buoys still have limitations to catch the full natural variability in global ocean due to their spatial or temporal coverage. Therefore, all three adjustment methods still have limitations in predicting the full natural variability, especially in dynamic systems. The comparison between VARbuoys and VARsocat shows that average VARbuoy was about two times the VARsocat in coastal and coral reef areas (Fig. 2). The Arctic Ocean is heavily impacted by recent sea-ice meltwater (Comiso et al., 2017; Qi et al., 2017), and neither SOCATv6 data nor buoy observations have enough Arctic coverage to validate or scale the modeled Arctic variability. Therefore, our YoE values based on the adjusted VARmodel should be treated with caution in coastal areas where complicated physical and biogeochemical processes exist, especially in the Arctic Ocean.

208 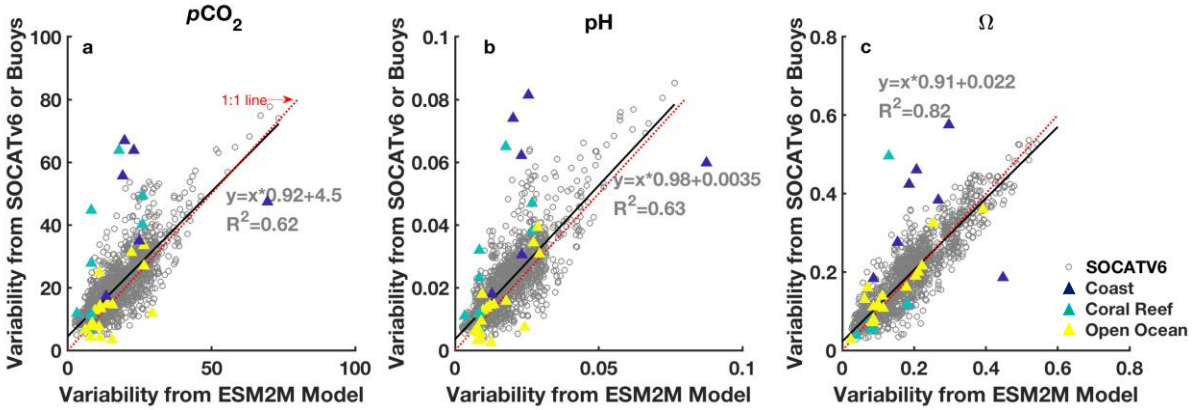

209 Fig. 2. The variability comparison among buoys (triangles), SOCATv6 (circle) and ESM2M
210 model for (a) pCO_2, (b) pH and (c) Ω. Yellow, cyan and blue triangles represent the buoys types
211 of open ocean, coral reef and coasts (see details in Sutton et al. (2019)). The insert straight lines
212 are the linear regress between ESM2M model and SOCATv6 based variability and red dashed
213 lines are 1:1 line. The grey equations are the fitted linear regression with R^2 for pCO_2, pH and Ω,
214 respectively. Note the regression outliers between ESM2M model and SOCATv6 have been
215 removed with criteria Cook's distance larger than three times the mean Cook's distance.

216 *4.2 Ocean Acidification Rates*

217 The historical ocean acidification rates from 1770 to 1870 are at least one magnitude lower
218 than the rates from 2020 to 2050 (Fig. 3). The modeled global pCO_2, pH and Ω trend from 2020
219 to 2050 is 3.67±0.17 µatm yr^{-1}, -0.0033±0.0005 yr^{-1}, and -0.012±0.003yr^{-1}, respectively. All rates
220 are faster than the observed ocean acidification rates in time series stations from 1980s to 2010s
221 (Bates et al, 2014: 1.89±0.60 µatm yr^{-1} for pCO_2, and -0.0018 ±0.0005 yr^{-1} for pH, -
222 0.0078±0.0030yr^{-1} for Ω).

ESM2M model data between 1770 and 1861 are based on the assumption that seawater CO_2 increased at the same rate as the atmospheric CO_2 everywhere in the global ocean. Therefore, ocean acidification rates from 1770 to 1870 are almost homogenously distributed across the global ocean, which is probably not the case in the real world. The future ocean acidification rates from 2020 to 2050 display a clear spatial distribution. For example, the slowest pCO_2 and pH changing rate from 2020 to 2050 are near the Equatorial Upwelling area, while maximum pH decrease rate is observed in high latitude (i.e., Arctic area) because the low buffer capacity (Jiang et al., 2019).

To the contrary, Ω declines from 2020 to 2050 are slowest in high latitude (Figs. 3, S8). The rate of Ω decline in tropical and temperate areas (between 40°S and 40°N) is 0.0141±0.002 yr^{-1}, which is significantly faster than rates in other areas (0.0096±0.002 yr^{-1}). Even though Ω in warm waters is presently higher than that in colder waters, the faster rate of decrease in warm waters will expose calcifying species, such as coral reef forming organisms, to more severe ocean acidification threats in the near future. The mean Ω between 25°S and 25°N in 2020 is 3.53±0.23, so we will inevitably lose coral reef habitats in the coming decades when coral reefs shift from net carbonate accumulation to net carbonate loss around Ω~3.5 (Kleypas et al., 1999; Ricke et al., 2013). This suggests urgent action is needed to prevent further loss of coral reef habitats (Hoegh-Guldberg et al., 2007). Meanwhile, the tropical areas would have a smaller seasonal and spatial variability in terms of Ω because of small temperature variability (Fig. S10). Therefore, the predicted ocean acidification changes there will throw the organisms out of their comfort zone faster than at higher latitudes, where the larger seasonal variability may have prepared the organisms there to be better positioned to bigger changes.

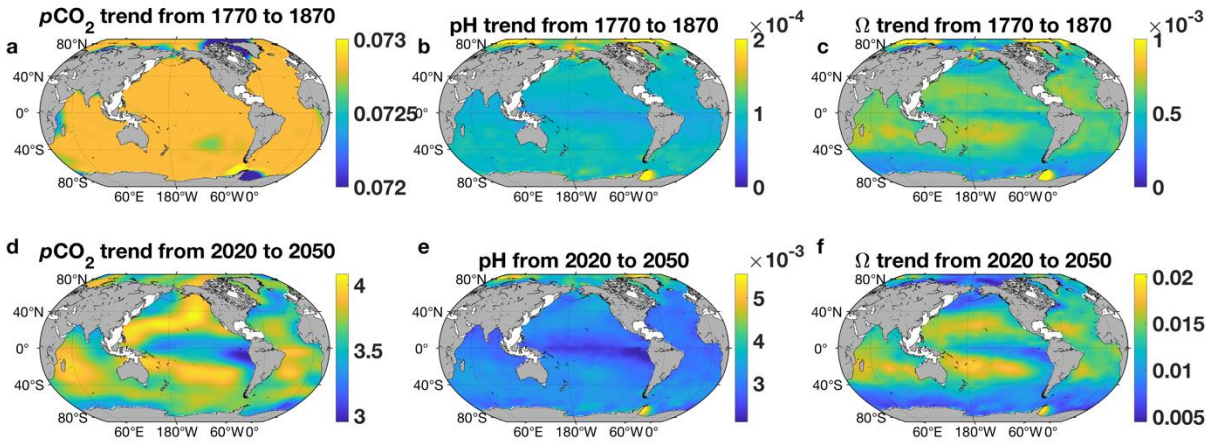

245

246 Fig. 3. Annual rates of ocean acidification showed by increasing pCO_2 (a, d), decreasing pH
247 (b, e), and decreasing Ω (c, f) distribution in historical period (1770 to 1870) and future (2020 to
248 2050) under the Intergovernmental Panel on Climate change RCP8.5 Scenario.

249 *4.3 Spatial Distributions of Year of Emergence*

250 The spatial distributions of YoEs show that pCO_2, pH and Ω have fully emerged from
251 preindustrial conditions before the 1950s in majority of the open ocean. This is true in the Indian
252 ocean, tropical Pacific and Atlantic Ocean, and the Southern Ocean near 40°S, but not yet the
253 case in some ocean margins (Figs. 4a, b c, Fig. 5, Table 1). As YoEs reflect the ratio between
254 natural variability and change rate from year 1770 to the YoE, the smaller internal variability in
255 open ocean than coastal areas and the almost homogenous open ocean acidification rates make
256 open oceans hotspots for emergence from historical conditions. For example, the tropical open
257 oceans broadly emerge before 1935. In addition, we calculated another two sets of *Noise* and
258 YoEs based on buoy variability adjustments (see: supplementary information) and found that
259 these varied YoE estimations have a similar spatial patterns and overall small disagreements in
260 global ocean (14~18 year deviations, Fig. S6). The average difference between YoEs (Method 2)

minus YoEs (Method 1) is 16 year for pCO_2, 17 year for pH, and 25 year for Ω, while the average difference between Method 3 minus Method 1 is 24 year for pCO_2, 22 year for pH, and 30 year for Ω. The difference reduces to 3~5 year for pCO_2/pH, and 8~12 year for Ω. As discussed in Section 4.1, the early YoEs in Arctic Ocean (before 1920, Figs. 3, 4) results from rapid modeled and SOCATv6 changes, but may be caused by the variability underestimation because the sparse training dataset in polar area in both SOCATv6 and buoys datasets.

There are also some coldspots for YoEs for all parameters, i.e., ocean margins from temperate to high latitude areas (20°N~60°N, Fig. 4), especially, the boundary current impacted areas in both Pacific and Atlantic, where the subseasonal and decadal variability can be especially significant (Carter et al., 2019). Taking the North Pacific for example, Kuroshio current shows well-defined decadal modulations between a stable and an unstable dynamic state, while Oyashio current and its extension area is accompanied by intense temperature and salinity fronts (Baolan et al., 2018; Qiu et al., 2017; Qiu et al., 2014). Overall, the presence of eddies, upwelling, and downwelling makes the hydrographic structure and biogeochemical parameters in such boundary currents more variable. This leads to much later YoEs than other areas for all parameters. For example, the YoE of Ω in the North Pacific and North Atlantic is at least 50 years later than (Figs. 4 and 5, Table 1). There are also very late YoEs for Ω in the upwelling region off Peru where the strength of upwelling is strongly modulated by decadal variability (i.e., El Niño Southern Oscillation).

The spatial pattern of ToE_2020s almost mimics the distribution of YoEs except the absolute years are different. The faster emergence of ocean acidification from present states are caused by the much higher future ocean acidification rates than in the historical period (Fig. 2).

Taking pCO_2 for example, the future trend from 2020 to 2050 is about 50 times as the historical trend, leading to a future emergence time that is one fiftieth as long. The spatial distribution of ToE_2020s are impacted by both the natural variability and ocean acidification rates from 2020 to 2050. In 95% of grid cells the ToE_2020s will emerge from the present state before year 2040 for pCO_2 and pH, and before year 2060 for Ω (Figs. 4 and 5). The exceptions are near the Bering Sea, south of 60°S, and within areas impacted by western boundary currents where all there is elevated natural variability. For example, northern latitudes between 30°N to 66°N that are affected by strong boundary currents (Kuroshio currents, and Gulf of Stream) are characterized by substantially later ToE_2020s for Ω (~2100, Figs. 4 and 5). In addition, both the low ocean acidification rates (Fig. 2) and high internal variability (Fig. S10) in Pacific Equatorial Upwelling are the reasons for the later ToE_2020s between 20°S and the equator for all three properties considered than in other open ocean areas (Figs. 4d, e, f). The Falkland current impacted area also has a longer ToE_2020s, which may be due to the higher variability caused by biological cycling or (and) decadal variability.

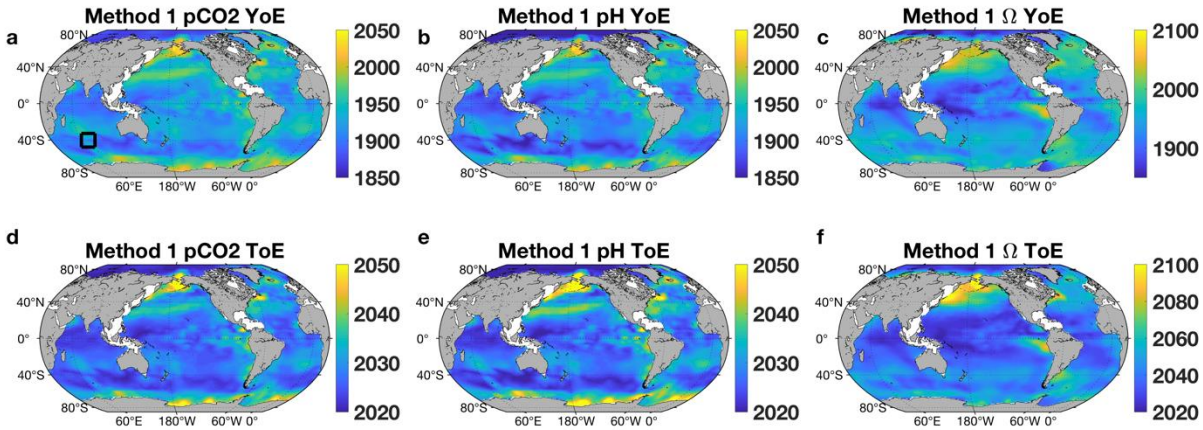

298 Fig. 4. Year and time of emergence distributions for pCO_2 (a, d), pH (b, e), and Ω (c, f)
299 based on variability adjustment by SOCATv6. The top panels are year of emergence from
300 preindustrial conditions (year 1770), and the bottom panels are the times of emergence from
301 present (year 2020). The colorbars for top and bottom panels are different. The square in panel a
302 show the location of example grid in Fig. 1.

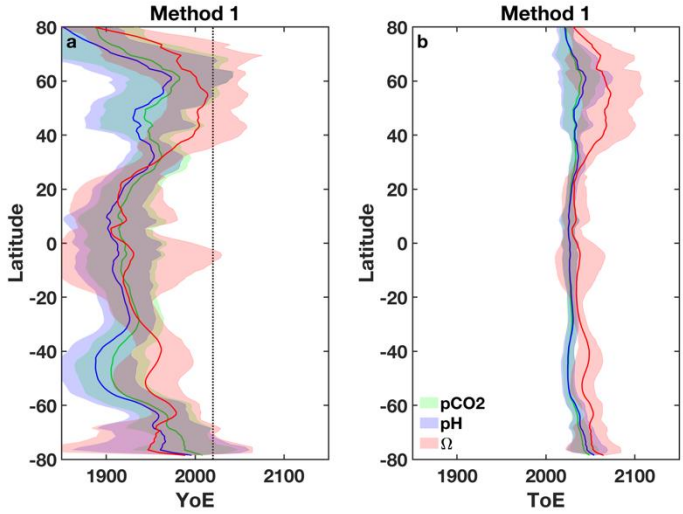

303

304 Fig. 5. The spatial distributions of (a) year of emergence from preindustrial conditions (year
305 1770) and (b) times of emergence from present (year 2020) for pCO_2 (red), pH (purple) and Ω
306 (green) along latitudinal bands (80°S to 80°N). The shades show the ranges of two times of
307 standard deviation in each latitudinal band. The insert dashed line in panel a shows year 2020.

308 Table 1. YoEs and ToEs (mean± standard deviation) in subregions for pCO_2, pH and Ω using
309 adjusted ESM2M model based on relationship between SOCATv6-based variability and ESM2M
310 model -based variability.

Subregion	Definition	YoEs			ToEs		
		pCO_2	pH	Ω	pCO_2	pH	Ω
Arctic Ocean	North of 66°N	1903±30	1874±32	1920±30	2025±5	2025±6	2041±9
North Pacific	66°N to 30°N	1973±18	1963±20	2007±19	2038±5	2043±7	2075±11

North Atlantic	66°N to 30°N	1952±18	1941±19	1986±13	2032±4	2034±5	2054±7
Tropical Pacific	30°N to 30 °S	1932±13	1924±13	1935±21	2029±2	2030±3	2037±6
Tropical Atlantic	30°N to 30 °S	1928±13	1919±13	1921±21	2028±2	2029±3	2034±6
Indian Ocean	North of 30°S	1912±10	1901±11	1924±19	2026±1	2026±2	2036±4
Southern Ocean	Southern of 30 °S	1941±19	1925±23	1957±23	2031±4	2033±5	2048±7

311

312 *4.4 Year of Emergence Comparison for Carbonate System Parameters*

313 Even though the ToE_2020s of pH average one year later than those for pCO_2, YoEs for pH
314 are significantly earlier (average of ~14 years) than YoEs for pCO_2 (Fig. 4). This finding differs
315 from a previous study that found that anthropogenic pCO_2 and pH changes emerged at same time
316 based on observations over a short time period (Sutton et al., 2019). Given that we used the same
317 set of *Noise* for both calculations, biases in *Noise* estimation (if there is any) over any time series
318 should have the same impact on YoEs and ToE_2020s on pCO_2 (or pH). Therefore, the delayed
319 YoEs for pH over time comparing to pCO_2 can only be caused by a decreasing rate of decline in
320 pH over such a long-time scale (1770 to 2050). This can be explained by noting that pH is on a
321 $\log_{10}$ scale, so it does not linearly change when the carbonate systems changes. Assuming total
322 alkalinity (A_T), salinity, and temperature are constant at 2400 µmol kg^{-1}, 35 and 20°C, then the
323 increasing pCO_2 from 280 to 290 µatm would decrease pH from 8.1875 to 8.1753 (delta=0.0122),
324 but pH only decreases from 8.0798 to 8.0705 (delta=0.0093) when pCO_2 increases from 380 to
325 390 µatm. Thus, the pH change rate is reduced by 23.3% with the same pCO_2 increase at higher
326 initial pCO_2. By contrast, $[H^+]$ differences under these two scenarios only decrease by 2%. The
327 surface ocean is therefore already in a meaningfully different condition today from how it was in
328 the preindustrial period, making the modern rate of pH change slower than the historical rate of
329 pH change with the same amount of pCO_2 increase (even though the rate of accumulation of $[H^+]$
330 is almost the same for a given pCO_2 change). Naturally, this non-linearity in pH may also

challenge assumption that *Noise* is static over time if H^+ variability is more stable over time than pH variability.

The global distributions of YoEs and ToE_2020s show that Ω has later emergences than other two carbonate parameters (Figs. 3, 4). The average YoE difference between Ω and pCO_2 (or pH) in global scale is 14~28 years ($P<0.001$), and the difference of ToE_2020s between Ω and pCO_2 (or pH) is 15~16 years ($p<0.001$). The later YoEs of Ω are caused by both higher natural variability and smaller change rates for Ω than for pCO_2 and pH. We examined the sensitivity of carbonate system to increasing pCO_2 (2 µatm yr^{-1}) in CO2SYS by assuming constant A_T and salinity at 2400 µmol kg^{-1} and 35, respectively. To simplify the natural variability of pCO_2, we used an arbitrarily selected pCO_2 variability (±20.5 µatm, 1 standard deviation) and started a trend at 280 µatm from year 0 (Scenario 1). YoEs could be determined with the simulated variability and temporal change rates of interested parameters (Fig. 5). The YoE sensitivity to global warming or temperature variability was further examined by assigning a warming rate (0.02°C yr^{-1}, Figs. 6c and d, Scenario 2) on basis of Scenario 1, or a random distribution for temperature reflecting natural variability (e.g., seasonality) in temperature (mu=20 °C, signal=2°C, Figs. 6e and f, Scenario 3) on basis of Scenario 1. Each simulation is run 180 times.

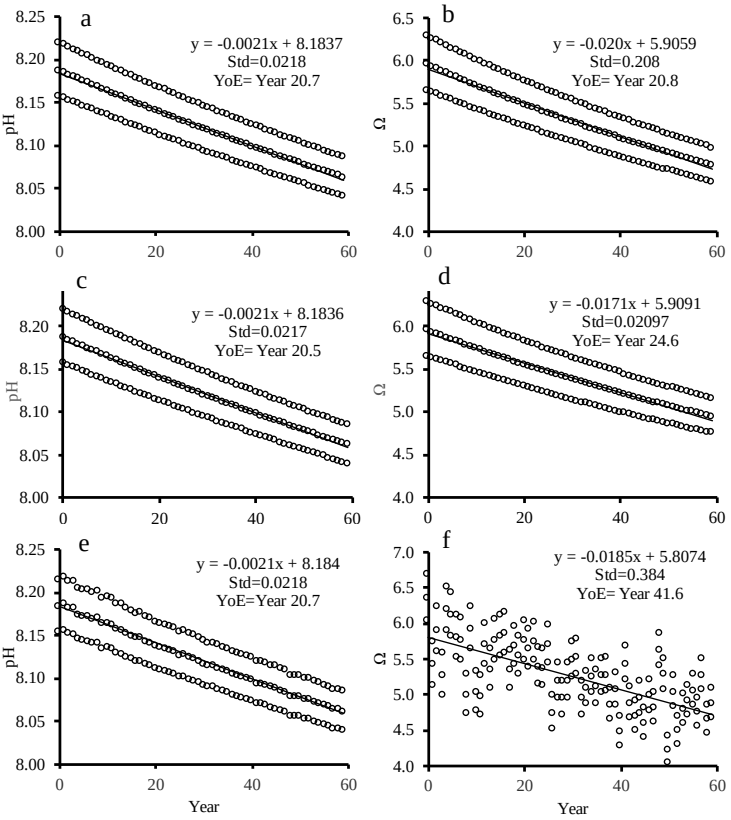

348

349 Fig. 6. (a) pH and (b) Ω changes in a simulation with a fixed pCO_2 *Noise* (±20.5 µatm, 1
350 standard deviation), A_T=2400 µmol kg^{-1}, salinity=35, temperature=20°C (Scenario 1); (c, d) are
351 similar calculations but with temperature increasing at rate of 0.02°C yr^{-1} (Scenario 2); and (e, f)
352 are similar calculations but with a temperature equaling 20°C ± 2°C (1 standard deviation)
353 (Scenario 3). All three scenarios have the same pCO_2 increase rate (2 µatm yr^{-1}). The middle
354 series of dots in each panel is the mean values with the higher and lower series representing the ±
355 the *Noise*. All calculates were done using CO2SYS. The regression equation, standard deviation
356 of detrended data, and YoEs (which can be thought of as the year when the center series has
357 changed by twice the *Noise*) are included in each panel.

358 YoEs for pCO_2 for all three scenarios are the same (year 20.5), because of the same rates of
359 pCO_2 increase and identical *Noise*. Though the absolute rates and variabilities are different

among pCO_2, pH, and Ω, their YoEs are all the same (20.5~20.8 year, Figs. 6a and b) when there is only pCO_2 increase. Therefore, the absorption of anthropogenic CO_2 has the same impact on the YoEs of pCO_2, pH and Ω, resulting from a fixed ratio between internal variabilities and ocean acidification rates caused by pCO_2 increases only. The YoEs of pH does not significantly change after adding a warming rate or a random temperature change (Figs. 6c and e). However, YoEs of Ω delays from year 20.8 year to year 24.6 when there is a warming rate of 0.02°C yr^{-1} (Fig. 6d), and reaches to year 33.5 when the warming rate is as high as 0.05 °C yr^{-1} (not shown). This elevated warming rate is expected to take place in coming decades in some tropical and Arctic areas (Fig. S10). The YoEs of Ω delays to year 41.6 when there is a 2°C random temperature change (Fig. 6f) due to greatly enhanced Ω *Noise* with a variable temperature (at fixed pCO_2). The standard deviation of SST in western boundary current regions falls in the range of 2°C to 5°C (Fig. S10), thus, a more delayed YoEs for Ω is expected there.

In summary, global warming can both slow down the Ω decrease rate and temperature variability can greatly increase the natural variability of Ω. Ω's temperature sensitivity can be explained with following three reasons (Carter et al., 2014; Jiang et al., 2015). First, the net equation of CO_2 dissolution and reaction is $CO_2+H_2O+CO_3^{2-}\leftrightarrow 2HCO_3^-$. This equilibrium would shift to left when temperature increases, leading to increases in carbonate ion concentration and Ω. Second, DIC degassing would also be enhanced when temperature increases, moving the acid-base equilibrium to the left. Third, the apparent solubility product (K'_{sp}) is negatively temperature dependent. Thus, Ω would increase when temperature increases. Global warming is a negative feedback for this aspect of climate change (Keller et al., 2014), thus, temperature independence leads to a delayed YoEs for Ω compared to pCO_2 and pH. In other words, it would take longer for Ω to emerge from the natural envelope compared to surface ocean pCO_2 or pH.

Future experimental designs must account for the biological impacts of ocean acidification from perspective of pCO_2 and pH, because these two parameters will fall out its natural variability sooner.

4.5. Further thoughts

Areas with early YoEs, such as in the open ocean, require attention because the biological communities need to acclimate to abnormal conditions sooner. However, YoEs cannot be assumed to equal the time at which biological thresholds will be crossed, particularly because organisms living in highly variable regions with later YoEs may already be stressed by the variability of their habitat. The combined effect of high natural variability and anthropogenic change may push the environment beyond biological thresholds more quickly (a shorter time to biological threshold may be expected instead). The impact of ocean acidification on biological systems need a more exhaustive examination in the future.

YoEs here only represent a theoretical period to expect anthropogenic signal emergence from natural variability. Local-scale human-imposed stresses (terrestrial nutrient inputs), and physical processes changes (e.g., upwelling or downwelling) can all mute or amplify the global-scale anthropogenic signals and change the ToEs in future. For example, Wang et al. (2017) suggested that enhanced upwelling may have led to a faster fCO_2 trend in the past decades compared to the rate of change in atmosphere. The *in situ* trends in coastal areas, which are heavily impacted by anthropogenic forcing, may significantly deviate from the modelled trends that do not parameterize for all human impacts. For example, the long-term alkalinity changes and on-going eutrophication in the Baltic Sea have partially or entirely counteracted the anthropogenic CO_2-induced ocean acidification (Laruelle et al., 2018; Müller et al., 2016).

Further studies need to confirm whether the local trends will persist at a constant rate or change in the context of climate change.

5. Conclusions

YoE is the first year when an anthropogenic signal exceeds the envelope of natural variability around the initial conditions. With aid of SOCATv6 and moored buoy-based variability, we scaled model-based variability across the global ocean to estimate YoEs globally using three different methods, yielding qualitatively similar estimates each time. Ocean acidification had fully emerged from preindustrial conditions in the vast open ocean before the 1950s, but will not have emerged until around 2050 in some ocean margins. Because the future ocean acidification rates from 2020 to 2050 are significantly faster than the historical ocean acidification rates from 1770s to 1870s, the ~95% of the global surface ocean will experience another new state from present before 2040 for pCO_2 and pH, and before 2060 for Ω. YoEs for pCO_2 and pH are earlier than for Ω due to the impacts of global warming and natural temperature variability on Ω trends and natural variability, respectively. Coastal areas that are heavily impacted by western boundary currents are coldspots for trend emergence. Continuous data collection and interpretation is necessary to study the impact of global-scale ocean acidification on ecosystem health in future.

6. Acknowledgements and data

HW wants to thank B. Yang from University of Virginia for teaching process satellite SST. We also want to thank T. Ono from Fisheries Oceanography Group, Oceanic resources Division for his helpful suggestions when forming the early draft. W-J. C acknowledges supports from

NOAA's Ocean Acidification Program. The 6th version of the Surface Ocean CO2 Atlas (SOCATv6) are at National Oceanic and Atmospheric Administration (NOAA) National Centers for Environmental Information (NCEI, DOI:10.7289/V51Z42R8). The climatological distributions of global surface ocean pH in all 12 months of the year from 1770 to 2100 are available through NOAA/NCEI (DOI: 10.25921/kgqr-9h49). Autonomous seawater pCO_2 and pH time series from 40 surface buoys are available at https://doi.org/10.7289/V5DB8043. Data archiving for the data products of this study, i.e., three sets of global variabilities of pCO_2, pH and aragonite saturation states (gridded data in mat format) is underway. The data products are included as supplements for review purposes.

7. Reference

Amante, C., & Eakins, B. W., 2009, ETOPO1 1 Arc-Minute Global Relief Model: Procedures, Data Sources and Analysis, NOAA Technical Memorandum NESDIS NGDC-24, National Geophysical Data Center, N.,

Baolan, W., Xiaopei, L., & Bo, Q. (2018). Meridional shift of the Oyashio Extension front in the past 36 years, *Geophysical Research Letters*, *45*, 9042-9048. 10.1029/2018GL078433

Bates, N., Astor, Y., Church, M., Currie, K., Dore, J., Gonaález-Dávila, M., et al. (2014). A time-series view of changing ocean chemistry due to ocean uptake of anthropogenic CO_2 and ocean acidification, *Oceanography*, *27*(1), 126-141. 10.5670/oceanog.2014.16

Carter, B., Toggweiler, J., Key, R., & Sarmiento, J. (2014). Processes determining the marine alkalinity and calcium carbonate saturation state distributions, *Biogeosciences*, *11*(24), 7349-7362. 10.5194/bg-11-7349-2014

Carter, B. R., Feely, R. A., Williams, N. L., Dickson, A. G., Fong, M. B., & Takeshita, Y. (2017). Updated methods for global locally interpolated estimation of alkalinity, pH, and nitrate, *Limnology and Oceanography: Methods*, *16*(2), 119-131. 10.1002/lom3.10232

Carter, B. R., Williams, N. L., Evans, W., Fassbender, A. J., Barbero, L., Hauri, C., et al. (2019). Time of Detection as a Metric for Prioritizing Between Climate Observation Quality, Frequency, and Duration, *Geophysical Research Letters*, *46*(7), 3853-3861. 10.1029/2018GL080773

Comiso, J. C., Meier, W. N., & Gersten, R. (2017). Variability and trends in the Arctic Sea ice cover: Results from different techniques, *Journal of Geophysical Research: Oceans*, *122*(8), 6883-6900. doi:10.1002/2017JC012768

Crompton, R. P., Pielke Jr, R. A., & McAneney, K. J. (2011). Emergence timescales for detection of anthropogenic climate change in US tropical cyclone loss data, *Environmental Research Letters*, *6*(1), 014003. 10.1088/1748-9326/6/1/014003

Feely, R. A., Doney, S. C., & Cooley, S. R. (2009). Ocean acidification: present conditions and future changes in a high-CO_2 world, *Oceanography*, *22*(4), 36-47. 10.5670/oceanog.2009.95

Friedrich, T., Timmermann, A., Abe-Ouchi, A., Bates, N., Chikamoto, M., Church, M., et al. (2012). Detecting regional anthropogenic trends in ocean acidification against natural variability, *2*(3), 167. 10.1038/nclimate1372

Giorgi, F., & Bi, X. (2009). Time of emergence (TOE) of GHG-forced precipitation change hot-spots, *Geophysical Research Letters*, *36*(6), L06709. 10.1029/2009GL037593

Hawkins, E., & Sutton, R. (2012). Time of emergence of climate signals, *Geophysical Research Letters*, *39*(1), L01702. 10.1029/2011GL050087

Henson, S. A., Beaulieu, C., Ilyina, T., John, J. G., Long, M., Séférian, R., et al. (2017). Rapid emergence of climate change in environmental drivers of marine ecosystems, *Nature communications*, *8*, 14682. 10.1038/ncomms14682

Hoegh-Guldberg, O., Mumby, P. J., Hooten, A. J., Steneck, R. S., Greenfield, P., Gomez, E., et al. (2007). Coral reefs under rapid climate change and ocean acidification, *Science*, *318*(5857), 1737-1742. 10.1126/science.1152509

Jiang, L.-Q., Carter, B. R., Feely, R. A., Lauvset, S. K., & Olsen, A. (2019). Surface ocean pH and buffer capacity: past, present and future, *Scientific Reports*, *9*(1), 18624. 10.1038/s41598-019-55039-4

Jiang, L.-Q., Feely, R. A., Carter, B. R., Greeley, D. J., Gledhill, D. K., & Arzayus, K. M. (2015). Climatological distribution of aragonite saturation state in the global oceans, *Global Biogeochemical Cycles*, *29*(10), 1656-1673. 10.1002/2015GB005198

Keller, K. M., Joos, F., & Raible, C. (2014). Time of emergence of trends in ocean biogeochemistry, *Biogeosciences*, *11*(13), 3647-3659. 10.5194/bg-11-3647-2014

Kleypas, J. A., McManus, J. W., & Menez, L. A. B. (1999). Environmental limits to coral reef development: Where do we draw the line?1, *American Zoologist*, *39*(1), 146-159. 10.1093/icb/39.1.146

Landschützer, P., Gruber, N., Bakker, D. C. E., Stemmler, I., & Six, K. D. (2018). Strengthening seasonal marine CO2 variations due to increasing atmospheric CO_2, *Nature Climate Change*. 10.1038/s41558-017-0057-x

Laruelle, G. G., Cai, W.-J., Hu, X., Gruber, N., Mackenzie, F. T., & Regnier, P. (2018). Continental shelves as a variable but increasing global sink for atmospheric carbon dioxide, *Nature Communications*, *9*(1), 454. 10.1038/s41467-017-02738-z

Lee, D., Min, S.-K., Park, C., Suh, M.-S., Ahn, J.-B., Cha, D.-H., et al. (2016). Time of emergence of anthropogenic warming signals in the Northeast Asia assessed from multi-regional climate models, *Asia-Pacific Journal of Atmospheric Sciences*, *52*(2), 129-137. 10.1007/s13143-016-0014-z

Lyu, K., Zhang, X., Church, J. A., Slangen, A. B., & Hu, J. (2014). Time of emergence for regional sea-level change, *Nature Climate Change*, *4*(11), 1006. 10.1038/nclimate2397

Müller, J. D., Schneider, B., & Rehder, G. (2016). Long-term alkalinity trends in the Baltic Sea and their implications for CO_2-induced acidification, *Limnology and Oceanography*, *61*(6), 1984-2002. 10.1002/lno.10349

Qi, D., Chen, L., Chen, B., Gao, Z., Zhong, W., Feely, Richard A., et al. (2017). Increase in acidifying water in the western Arctic Ocean, *Nature Climate Change*, *7*, 195. 10.1038/nclimate3228

Qiu, B., Chen, S., & Schneider, N. (2017). Dynamical links between the decadal variability of the Oyashio and Kuroshio extensions, *Journal of Climate*, *30*(23), 9591-9605. 10.1175/JCLI-D-17-0397.1

Qiu, B., Chen, S., Schneider, N., & Taguchi, B. (2014). A coupled decadal prediction of the dynamic state of the Kuroshio Extension system, *Journal of Climate*, *27*(4), 1751-1764. 10.1175/JCLI-D-13-00318.1

Ricke, K. L., Orr, J. C., Schneider, K., & Caldeira, K. (2013). Risks to coral reefs from ocean carbonate chemistry changes in recent earth system model projections, *Environmental Research Letters*, *8*(3), 034003. 10.1088/1748-9326/8/3/034003

Sui, Y., Lang, X., & Jiang, D. (2014). Time of emergence of climate signals over China under the RCP4.5 scenario, *Climatic Change*, *125*(2), 265-276. 10.1007/s10584-014-1151-y

Sutton, A. J., Feely, R. A., Maenner-Jones, S., Musielwicz, S., Osborne, J., Dietrich, C., et al. (2019). Autonomous seawater pCO_2 and pH time series from 40 surface buoys and the emergence of anthropogenic trends, *Earth Syst. Sci. Data*, *11*(1), 421-439. 10.5194/essd-11-421-2019

Sutton, A. J., Sabine, C. L., Feely, R. A., Cai, W. J., Cronin, M. F., McPhaden, M. J., et al. (2016). Using present-day observations to detect when anthropogenic change forces surface ocean carbonate chemistry outside preindustrial bounds, *Biogeosciences*, *13*(17), 5065-5083. 10.5194/bg-13-5065-2016

Turk, D., Wang, H., Hu, X., Gledhill, D. K., Wang, Z. A., Jiang, L., & Cai, W.-J. (2019). Time of emergence of surface ocean carbon dioxide trends in the North American coastal margins in support of ocean acidification observing system design, *Frontier Marine Science*, *6*, 91. 10.3389/fmars.2019.00091

van Heuven, S., D. Pierrot, J.W.B. Rae, E. Lewis, and D.W.R. Wallace (2011). MATLAB Program Developed for CO_2 System Calculations, *Oak Ridge, Tennessee*. 10.3334/CDIAC/otg.CO2SYS_MATLAB_v1.

Wang, H., Hu, X., Cai, W.-J., & Sterba-Boatwright, B. (2017). Decadal fCO_2 trends in global ocean margins and adjacent boundary current-influenced areas, *Geophysical Research Letters*, *44*, 8962–8970. 10.1002/2017GL074724

Zeebe, R. E., & Wolf-Gladrow, D. A. (2001). *CO_2 in seawater: equilibrium, kinetics, isotopes*, 7-8 pp., Gulf Professional Publishing.